Superoxide Radical Anion Adduct of 5,5-Dimethyl-1-pyrroline *N*-Oxide. 4. Conformational Effects on the EPR Hyperfine Splitting Constants

Frederick A. Villamena,*,†,‡ Yangping Liu,‡ and Jay L. Zweier‡

Department of Pharmacology and Center for Biomedical EPR Spectroscopy and Imaging, The Davis Heart and Lung Research Institute, and the Division of Cardiovascular Medicine, Department of Internal Medicine, College of Medicine, The Ohio State University, Columbus, Ohio 43210

Received: August 7, 2008; Revised Manuscript Received: October 6, 2008

Spin trapping has been commonly employed in the detection of superoxide radical anion in chemical and biological systems; hence, accurate interpretation of the hyperfine splitting constants (hfsc's) arising from the $O_2^{\bullet-}$ adducts (also referred to as hydroperoxyl ($HO_2^{\bullet}$) radical adducts) of various nitrones is important. In this work, the nature of the relevant hfsc's was investigated by examining the effect of conformational changes in the hydroperoxyl moiety of the $O_2^{\bullet-}$ adducts of 5,5-dimethyl-1-pyrroline *N*-oxide (DMPO), 5-ethoxycarbonyl-5-methyl-1-pyrroline *N*-oxide (EMPO), 5-diethoxyphosphoryl-5-methyl-1-pyrroline *N*-oxide (DEPMPO), 5-carbamoyl-5-methyl-1-pyrroline *N*-oxide (AMPO), and 7-oxa-1-azaspiro[4.4]non-1-en-6-one *N*-oxide, (CPCOMPO) on the magnitude of a_N, $a_{\beta\text{-H}}$, and $a_{\gamma\text{-H}}$. Conformational change around the substituents and their effect on the hfsc's were also explored. Results indicate that $a_{\beta\text{-H}}$ is most sensitive to conformational changes of the hydroperoxyl and substituent groups relative to hfsc's of other nuclei. The orbital overlap between the C−H σ-orbital and the SOMO of the nitroxyl nitrogen plays a crucial factor in determining the magnitude of the $a_{\beta\text{-H}}$. The hfsc values for the $O_2^{\bullet-}$ adducts were predicted with high accuracy by using a low-cost computational method at the PCM(water)/BHandHLYP/EPR-III//B3LYP/6-31G* level of theory without taking into account the explicit water interaction.

I. Introduction

Identification of free radicals in chemical and biological systems has been possible through the use of nitrone spin traps and electron paramagnetic resonance (EPR) spectroscopy.[1] Spin trapping has found enormous application in the field of biomedical research, particularly in the study of the toxicology of free radicals[2] and the crucial role they play in regulating cell function.[3] Moreover, the use of spin trapping has been gaining popularity in the investigation of reactive intermediates in the areas of fuel cell research,[4] nanotechnology,[5] catalysis,[6] environmental remediation,[7] and photodynamic therapy.[8] Among the most commonly studied radicals are the hydroxyl radical ($HO^{\bullet}$) and superoxide radical anion ($O_2^{\bullet-}$), using the cyclic nitrones, 5,5-dimethyl-1-pyrroline *N*-oxide (DMPO),[9] 5-ethoxycarbonyl-5-methyl-1-pyrroline *N*-oxide (EMPO),[10] and 5-diethoxyphosphoryl-5-methyl-1-pyrroline *N*-oxide (DEPMPO)[11] (Scheme 1), even though the use of these spin traps is still confronted by some limitations such as slow reactivity to $O_2^{\bullet-}$ and generally less persistent $O_2^{\bullet-}$ adducts. The detection of $O_2^{\bullet-}$ in in vitro and in vivo systems has attracted considerable attention over the past 2 decades due to the important role that $O_2^{\bullet-}$ plays in cell signaling and immune response.[12] Superoxide radical anion has also been shown to be a major source of the most highly reactive species known to exist in biological systems such as $HO^{\bullet}$, peroxynitrite, carbonate radical anion, oxidized glutathione radical anion, and hypochlorous acid, all of which have been implicated in the pathogenesis of various diseases.[13]

SCHEME 1: Spin Trapping of Superoxide Radical Anion by Cyclic Nitrones

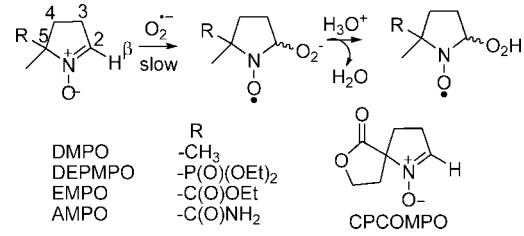

Due to the importance of identifying $O_2^{\bullet-}$ from biological systems, there is therefore a pressing need to develop innovative spin traps with improved spin trapping properties. Our systematic approach to spin trap development using computational methods[14−18] in the analysis of the spin trapping processes has led to the prediction and synthesis of novel nitrones with improved properties.[19,20] Aside from the challenges that have to be overcome in the design of new spin traps, e.g., the slow reactivity of nitrones to $O_2^{\bullet-}$ and fast adduct decay rate, it is equally important to synthesize spin traps that can exhibit discernible EPR spectra which make spin trapping a unique technique for radical identification. It will be an important advancement in the field of spin trapping if EPR parameters, particularly the hyperfine splitting constants (hfsc, a_x), can be predicted such that it will be possible to simulate EPR spectra of spin adducts by using quantum mechanical approximations even before the adduct is experimentally generated. It is therefore of critical importance to fully understand the nature of the experimentally observed hfsc's, especially those of the $O_2^{\bullet-}$ adduct of the commonly used cyclic nitrones, and to predict the relevant hfsc by using a low-cost computational method at first approximation.

* Corresponding author. E-mail: frederick.villamena@osumc.edu. Fax: 614-688-0999.
† Department of Pharmacology.
‡ Center for Biomedical EPR Spectroscopy and Imaging.

10.1021/jp8070579 CCC: $40.75
Published on Web 11/14/2008

SCHEME 2: Chemical Structures of 2,2,5,5-Tetramethyl-3-carboxypyrroline (3-carboxy-PROXYL, CP) and 2,2,6,6-Tetramethyl-4-carboxypiperidine (4-carboxy-TEMPO, CT)

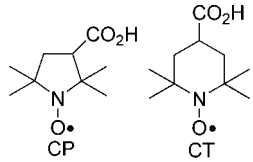

The EPR spectral analysis of the $O_2^{\bullet-}$ adduct of cyclic nitrones is complicated due to the presence of asymmetric line widths that are attributed to the presence of conformational exchanges within the molecule. The line width and hfsc profile become more complicated with the 5-substituted pyrroline *N*-oxides such as EMPO, DEPMPO, and more recently 5-carbamoyl-5-methyl-1-pyrroline *N*-oxide (AMPO)[19] and 7-oxa-1-azaspiro[4.4]non-1-en-6-one *N*-oxide (CPCOMPO),[20] due to the formation of diastereomeric species, since each species exhibits a distinctive EPR spectral profile (see Scheme 1). The interpretation of the EPR spectra of the $O_2^{\bullet-}$ adducts of DMPO and DEPMPO has been a subject of debate. Several investigators have applied synthesis of isotopically labeled DMPO,[21] EPR analysis,[22] and computational approaches[15,21,22] to interpret the nature of the EPR spectra of DMPO-O_2H arising from the γ-hydrogen. Moreover, assignment of the cis or trans isomer for the $O_2^{\bullet-}$ adducts of C-5 substituted cyclic nitrones, such as in the case of DEPMPO, has also been a major contention since extensive EPR analysis[23] indicates that the trans $O_2^{\bullet-}$ adduct is the major product but computational studies[18] show that the cis adduct is expected to be more thermodynamically and kinetically preferred due to the preference of $O_2^{\bullet-}$ addition at the cis position according to Scheme 1. Attempts to also rationalize the major diastereomeric product from kinetics of adduct decay, and calculated $a_N/a_{\beta\text{-H}}$ of the cis−trans isomeric products from CPCOMPO, also revealed that the cis isomer is the major $O_2^{\bullet-}$ adduct formed.[20] Although a_N values have been predicted with reasonable accuracy for tetramethyl-substituted nitroxides, CP and CT[24] (Scheme 2) and $O_2^{\bullet-}$ adducts of cyclic nitrones,[15,19,20] this has not been the case for $a_{\beta\text{-H}}$ even if the bulk dielectric effect of water and explicit water interaction have been considered in the calculation of the energetics of the adducts. Table 1 shows the various reported experimental and calculated hfsc's and the differences that exist between them. Since a_N and $a_{\beta\text{-H}}$ of $O_2^{\bullet-}$ adducts are major components of the spectra, it is imperative to thoroughly investigate the effect of conformational changes within the adduct structure on the magnitude of relevant hfsc's that give rise to unique fingerprintable spectral features.

II. Benchmark Studies

The mechanisms of superoxide adduct formation are shown in eqs 1 and 2 and the favorability of these reactions are pH dependent.[25] For example, the reactivity of $O_2^{\bullet-}$ to DMPO is slow, with a second order rate constant of only 2.0 M^{-1} s^{-1}; however, at acidic pH, the reactivity is ~27 or ~10^3 M^{-1} s^{-1} at pH 6.2 and 5.0,[9] respectively. The observed higher reactivity of $HO_2^{\bullet}$ to DMPO compared to $O_2^{\bullet-}$ was theoretically confirmed and the predicted rate constant in the aqueous phase for the $O_2^{\bullet-}$ [18] or $HO_2^{\bullet}$ [17] addition to DMPO was found to be 5.9 × 10^{-5} and 285 M^{-1} s^{-1}, respectively, at the PCM/B3LYP/6-31+G**//B3LYP/6-31G* level of theory. At neutral pH, although the addition of $O_2^{\bullet-}$ predominates over the addition of $HO_2^{\bullet}$ to nitrones ($pK_a(HO_2^{\bullet}) = 4.8$),[26] this initial $O_2^{\bullet-}$ addition to nitrones can ultimately lead to the formation of HO_2-adducts (eq 1),[18] since the calculated pK_a for DMPO-O_2H, for example, was ~15, similar to the pK_a values observed for water and alcohols.[16] Therefore, the observed spectra arising from the trapping of $O_2^{\bullet-}$ are due to the final adduct form, nitrone-O_2H.

TABLE 1: Reported Calculated and Experimental (in parentheses) Hyperfine Splitting Constants of the Superoxide Spin Adducts of Various Spin Traps[a]

		predicted hyperfine splitting constants (G)			
nitrone-O_2H adducts	isomers	a_N	$a_{\beta-H}$	$a_{\gamma-H}$	a_P
DMPO-O_2H[9]	n/a[b]	(14.3)	(11.7)	(1.3)	n/a[b]
DMPO-O_2H[15]	n/a[b]	10.7	9.3	1.8	n/a[b]
DMPO-O_2H[21]	n/a[b]	7.3	6.6	1.90	n/a[b]
EMPO-O_2H[38]	**I** (59%)	(13.1)	(11.7)	(n/a)[b]	(n/a)[b]
	II (41%)	(13.1)	(9.3)	(n/a)[b]	(n/a)[b]
EMPO-O_2H[19]		11.6	14.4	0.3	n/a[b]
AMPO-O_2H[19]	**I** (80%)	(13.0)	(10.8)	(n/a)[b]	(n/a)[b]
	II (20%)	(13.1)	(12.5)	(1.8)	(n/a)[b]
AMPO-O_2H[19]		12.5	14.5	1.9	n/a[b]
DEPMPO-O_2H[11]	**I** (50%)	(13.4)	(11.9)	(0.8)	(52.5)
	II (50%)	(13.2)	(10.3)	(0.9)	(48.5)
DEPMPO-O_2H[19]		11.8	6.7	1.0	43.9
CPCOMPO-O_2H[20]	**I** (62%)	(13.0)	(10.0)	(1.5)	n/a[b]
	II (17%)	(13.1)	(11.5)	(1.1)	n/a[b]
CPCOMPO-O_2H[20]	cis	10.5	6.8	n/a[b]	n/a[b]
	trans	11.7	8.2	n/a[b]	n/a[b]

[a] Calculated hyperfine splitting constants were obtained from the most stable conformation of each spin or from the Boltzmann average of various conformations. [b] Not available.

Therefore, the performance of various theoretical methods

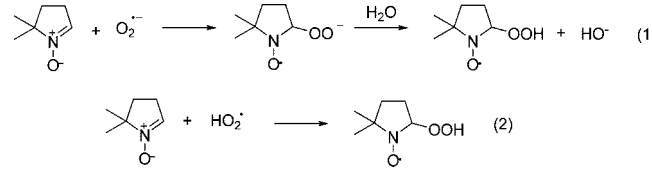

was assessed by calculation of the bottom-of-the-well energies ($\Delta E_{rxn,0K}$) for $HO_2^{\bullet}$ addition to nitrones as shown in eq 2. All calculations were performed with Gaussian 03[27] at the Ohio Supercomputer Center. The HF/cc-pVDZ, B3LYP/cc-pVDZ, B3LYP/6-31G*, mPW1K/6-31+G**, and B3LYP/cc-pVDZ//B3LYP/6-31G* levels of theory were within <0.5 kcal/mol energy difference from that obtained with CBS-QB3 (Table 2). On the basis of the similarity in predicted energetics for $HO_2^{\bullet}$ addition to nitrones with the use of B3LYP/6-31G* and CBS-QB3, the former could provide lower cost, yet accurate energies for $HO_2^{\bullet}$ addition reactions.

Single-point energy calculations using the BH and HLYP and ROMP2 methods, and B3LYP/6-31G* optimized geometries gave the least accurate energies contrary to that previously reported[28] for the prediction of energy barriers in which BHandHLYP provided good agreement with the highest levels of theory used in that study. Moreover, single-point energy calculations at the CCSD(T)/cc-pVDZ, CCSD/aug-cc-pVDZ, QCISD/cc-pVDZ, and QCISD/aug-cc-pVDZ levels of theory with the B3LYP/6-31G* optimized geometries gave 1.2−2.1 kcal/mol energy difference compared to that obtained with CBS-QB3. It is therefore reasonable to apply the B3LYP/6-31G* level of theory for the optimization of the various geometries of the spin adduct.

TABLE 2: Bottom-of-the-Well Reaction Energies ($\Delta E_{rxn,0K}$ in kcal/mol) for the Formation of DMPO-O_2H Calculated with Various Methods and Basis Sets

levels of theory	$\Delta E_{rxn,0K}$ (kcal/mol)
HF/cc-pVDZ	−30.7
MP2/cc-pVDZ	−33.6
B3LYP/cc-pVDZ	−30.1
B3LYP/6-311G**	−28.5
B3LYP/6-31G*	−30.7
B3LYP/aug-cc-pVDZ	−26.6
CBS-QB3	−30.6
BHandHLYP/6-311++G**	−32.5
BHandHLYP/6-311 g**	−34.3
BHandHLYP/aug-cc-pVDZ	−32.3
BHandHLYP/cc-pVDZ	−35.4
mPW1K/6-31+G**	−30.2
BHandHLYP/6-311 g**//B3LYP/6-31G*	−34.0
BHandHLYP/aug-cc-pVDZ//B3LYP/6-31G*	−31.8
BHandHLYP/cc-pVDZ//B3LYP/6-31G*	−35.0
CCSD(T)/cc-pVDZ//B3LYP/6-31G*	−31.8
CCSD/aug-cc-pVDZ //B3LYP/6-31G*	−31.7
QCISD/cc-pVDZ//B3LYP/6-31G*	−31.3
QCISD/aug-cc-pVDZ //B3LYP/6-31G*	−28.5
ROMP2/6-311G**//B3LYP/6-31G*	−57.9
ROMP2/aug-cc-pVDZ//B3LYP/6-31G*	−60.4
ROMP2/cc-pVDZ//B3LYP/6-31G*	−57.5
B3LYP/6-31+G**//B3LYP/6-31G*	−27.3
B3LYP/cc-pVDZ//B3LYP/6-31G*	−30.1
B3LYP/aug-cc-pVDZ //B3LYP/6-31G*	−26.6

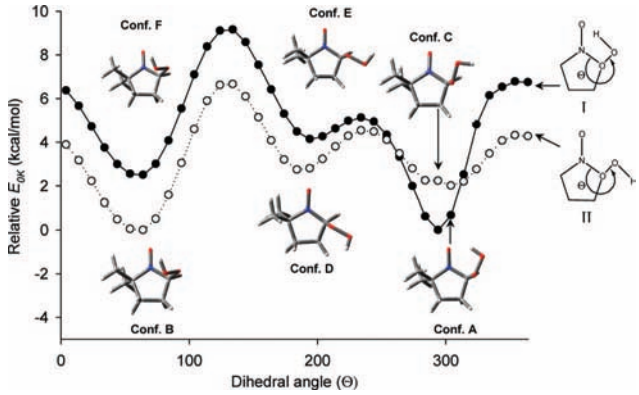

Figure 1. Potential energy plots at the B3LYP/6-31G* level of DMPO-O_2H conformations (I and II) showing the different minima as A, B, C, D, E, and F.

III. Conformational Search

Density functional theory[29] at the B3LYP/6-31G* level of theory was applied for the conformational search using the opt=modredundant keyword that allows a relaxed potential energy surface scan of the varying ∠N−C−O−O dihedral angle of the hydroperoxyl moiety (Figure 1). Hyperfine splitting constants were also obtained along with the potential energies for each dihedral angle (Figure 2). As shown in Figure 1, two major conformations were initially considered in which the −OH group of the hydroperoxyl moiety is pointing toward and away from the N−O group, and were assigned as conformers I and II, respectively. Potential energy plots of the various DMPO-O_2H conformations gave a total of 6 minima, i.e., conformations A−F (see Figure 1) consistent to that previously reported.[16] Optimized geometry and vibrational frequencies of all stationary points were obtained for the various minima at the B3LYP/6-31G* level of theory.[30] All adducts were determined to have zero imaginary vibrational frequencies as derived from a harmonic vibrational frequency analysis at the level at which the stationary points were optimized. For the minima,

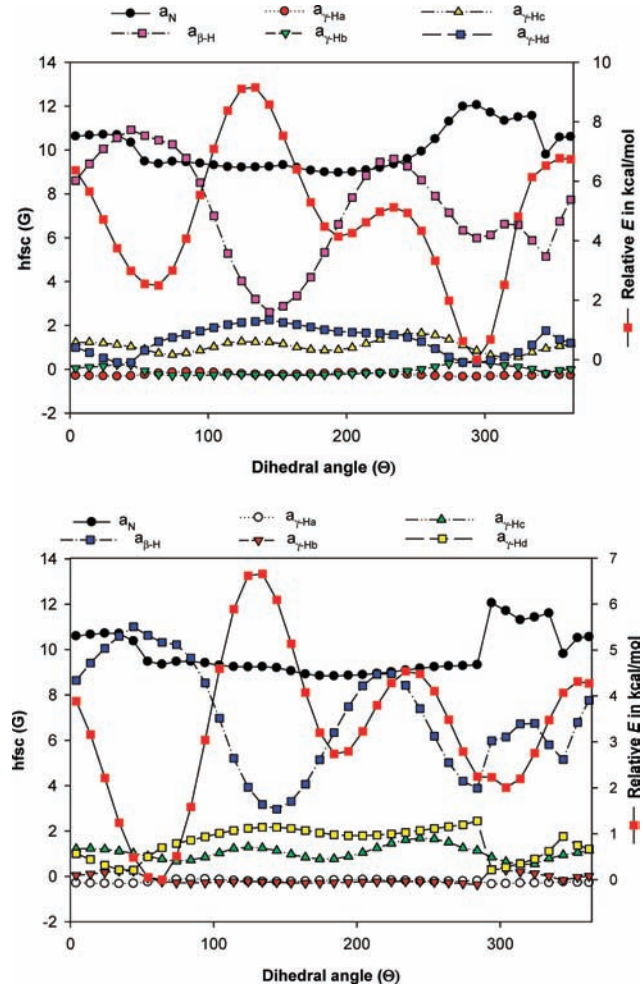

Figure 2. Conformational dependence of the hyperfine splitting constants (hfsc) of nitrogen, β-hydrogen, and γ-hydrogen atoms calculated at the B3LYP/6-31G* level of theory for conformations I-A (top) and II-B (bottom).

spin contamination values for the radical adducts are negligible, i.e., $0.75 < \langle S^2 \rangle < 0.80$. The optimized relative free energies ($G_{298K,gas}$) for each minimum at the B3LYP/6-31+G**//B3LYP/6-31G* level of theory were calculated and as follows (values in parentheses are relative free energies in aqueous phase, $G_{298K,aq}$ at the PCM/B3LYP/6-31+G**//B3LYP/6-31G* level), in kcal/mol: I-A, 0.0 (0.0); II-B, 1.0 (−3.0); II-C, 2.2 (−3.0); II-D, 2.8 (−2.3); I-E, 1.7 (−2.4); I-F, 1.0 (−3.0). Since I−F yielded a conformation similar to that of II-B, only five unique final conformations were obtained as I-A, II-B, II-C, II-D, and I-E with ∠N−C−O−O dihedral angles of 284.1°, 60.3°, 294.6°, 187.7°, and 185.7°, respectively.

IV. Prediction of Hyperfine Splitting Constants for DMPO-O_2H

a. Effect of Level of Theories. Comparison of the gas-phase energies of the various I and II DMPO-O_2H conformers at the B3LYP/6-31+G**//B3LYP/6-31G* level yielded conformation I-A as the most preferred isomer while II-B was the most favorable in aqueous phase at the PCM/B3LYP/6-31+G**//B3LYP/6-31G* level. Therefore, hyperfine splitting constants (hfsc's) at various levels of theory using B3LYP/6-31G* geometries of the DMPO-O_2H conformations I-A and II−B were obtained using gas- and aqueous-phase single-point calculations. The direct proportionality of the

TABLE 3: Gas-Phase Single Point Calculations of the Hyperfine Splitting Constants with B3LYP/6-31G* Geometries of the DMPO-O_2H Conformations I-A and II-B in the Gas Phase (values in parentheses are in the aqueous phase)

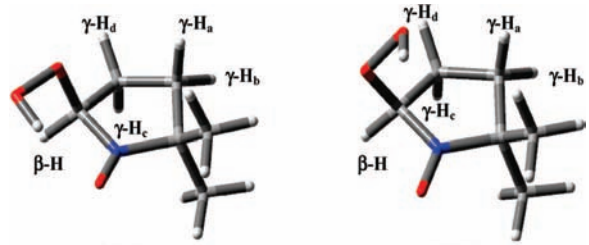

I-A II-B

methods	a_N	$a_{\beta\text{-H}}$	$a_{\gamma\text{-Ha}}$	$a_{\gamma\text{-Hb}}$	$a_{\gamma\text{-Hc}}$	$a_{\gamma\text{-Hd}}$
I-A						
B3LYP/6-31G*	12.0 (12.7)	6.5 (6.8)	−0.3 (−0.4)	0.4 (0.3)	1.1 (1.1)	0.4 (0.4)
B3LYP/6-31+G**	11.9 (14.3)	6.6 (6.9)	−0.3 (−0.3)	0.3 (0.2)	1.1 (1.1)	0.4 (0.5)
B3LYP/EPR-II	10.2 (11.0)	6.9 (7.3)	−0.3 (−0.4)	0.4 (0.3)	1.1 (1.2)	0.4 (0.5)
B3LYP/EPR-III	10.5 (11.3)	7.0 (7.3)	−0.4 (−0.4)	0.4 (0.3)	1.1 (1.2)	0.5 (0.5)
CISD/6-31+G**	21.3 (22.7)	6.9 (7.1)	−0.1 (−0.6)	0.1 (0.0)	0.6 (0.7)	−0.2 (−0.2)
CISD/EPR-II	18.0 (19.1)	6.8 (7.1)	−0.6 (−0.6)	0.1 (0.0)	0.7 (0.7)	−0.2 (−0.2)
PBE0/6-31+G**	13.8 (14.9)	6.5 (6.8)	−0.4 (−0.4)	0.3 (0.2)	1.0 (1.0)	0.3 (0.4)
PBE0/EPR-II	10.6 (11.5)	6.7 (7.0)	−0.4 (−0.4)	0.3 (0.3)	1.0 (1.0)	0.3 (0.4)
PBE0/ EPR-III	10.7 (11.6)	6.8 (7.1)	−0.4 (−0.4)	0.3 (0.3)	1.0 (1.1)	0.3 (0.4)
BHandHLYP/6-31+G**	15.8 (18.3)	6.7 (7.1)	−0.4 (−0.5)	0.2 (0.2)	0.8 (0.9)	0.1 (0.1)
BHandHLYP/EPR-II	14.9 (16.1)	6.9 (7.3)	−0.5 (−0.5)	0.2 (0.2)	0.8 (0.9)	0.1 (0.1)
BHandHLYP/EPR-III	15.0 (16.3)	7.0 (7.4)	−0.5 (−0.5)	0.3 (0.2)	0.9 (0.9)	0.1 (0.1)
II-B						
B3LYP/6-31G*	9.5 (10.9)	10.3 (11.1)	−0.2 (−0.3)	−0.2 (−0.3)	0.8 (0.7)	1.2 (1.1)
B3LYP/6-31+G**	9.5 (10.6)	10.4 (11.3)	−0.2 (−0.3)	−0.3 (−0.3)	0.8 (0.8)	1.2 (1.2)
B3LYP/EPR-II	7.8 (8.8)	11.1 (12.0)	−0.3 (−0.3)	−0.3 (−0.3)	0.8 (0.8)	1.3 (1.3)
B3LYP/EPR-III	8.1 (9.1)	11.2 (12.1)	−0.3 (−0.3)	0.2 (−0.3)	0.8 (0.8)	1.3 (1.3)
CISD/6-31+G**	17.9 (22.7)	10.2 (7.1)	−0.4 (−0.6)	−0.6 (0.0)	0.3 (0.7)	0.5 (−0.2)
CISD/EPR-II	14.4 (19.1)	10.2 (7.1)	−0.4 (−0.6)	−0.5 (0.0)	0.3 (0.7)	0.5 (−0.2)
PBE0/6-31+G**	11.3 (12.7)	10.4 (11.3)	−0.3 (−0.4)	−0.3 (−0.4)	0.7 (0.7)	1.1 (1.1)
PBE0/EPR-II	8.1 (9.1)	10.8 (11.6)	−0.3 (−0.4)	−0.3 (−0.4)	0.7 (0.7)	1.1 (1.1)
PBE0/ EPR-III	8.2 (9.3)	10.9 (11.8)	−0.3 (−0.4)	−0.3 (−0.4)	0.7 (0.7)	1.2 (1.2)
BHandHLYP/6-31+G**	14.1 (16.0)	10.3 (11.3)	−0.3 (−0.4)	−0.4 (−0.4)	0.5 (0.5)	0.8 (0.8)
BHandHLYP/EPR-II	11.8 (13.5)	10.7 (11.8)	−0.3 (−0.4)	−0.4 (−0.5)	0.5 (0.5)	0.8 (0.9)
BHandHLYP/EPR-III	12.1 (13.7)	10.8 (12.0)	−0.3 (−0.4)	−0.4 (−0.5)	0.6 (0.5)	0.9 (0.9)
exptl	**14.3**	**11.7**		**1.25**		

nuclear spin population (density) ρ_{rx} with the hfsc (a_X) is based on eq 3

$$a_X = 8\pi/3(g_e/g_0)\gamma_x\beta_x\rho_{rx} \quad (3)$$

where g_0 is the isotropic g-value for the radical, g_e the g-value for the free electron, γ_x the gyromagnetic nuclear ratio, and β_x the nuclear magneton of the nucleus X.[31] The calculated hfsc's for I-A and II-B are shown in Table 3 and in general, gas-phase hfsc values are lower than the aqueous phase hfsc's. Among the methods used for the prediction of a_N values in the gas phase, BHandHLYP gave the best approximations with use of the basis set EPR-II or EPR-III for both I-A and II-B but the $a_{\beta\text{-H}}$ values were only accurately predicted for the II-B conformer. In general, the B3LYP and PB0 methods gave underestimated hfsc's while the CISD method gave over approximated values in the gas phase. In the aqueous phase, the best approximations for a_N, $a_{\beta\text{-H}}$, and the $a_{\gamma\text{-Hd}}$ were also achieved for II-B with the BHandLYP method, using EPR-II and EPR-III basis sets.

b. Effect of Water Interaction. The effect of solvation on the predicted gas-phase hfsc was investigated via single-point energy calculations at various levels, using the polarizable continuum model (PCM) to represent water.[32] The effect of explicit water interaction on the predicted hfsc was also investigated through optimization of structures with two water molecules via initial conformational search, using Spartan 04[33] via a Monte Carlo method coupled with the MMFF-94 force field. Conformational search with initial structures for I-A, II-B, II-C, II-D, and I-E with 2 water molecules only yielded complexes with I-A and II-B type conformations. Structures of the most preferred conformations were further optimized at the B3LYP/6-31G* level of theory and single-point calculation at the PCM(water)/BHandHLYP/EPR-III level. Table 4 shows the various hfsc values of conformers I-A, II-B, II-C, II-D, and I-E in the gas and aqueous phases as well as in the presence of two explicit water molecules in aqueous phase for I-A and II-B. Results show that the presence of bulk dielectric effect of water increases the predicted hfsc's from the gas-phase hfsc's but not significantly in the presence of explicit water interaction. The predicted hfsc's are most accurate for the most preferred conformation, i.e. II-B with predicted a_N and $a_{\beta\text{-H}}$ of 13.7 and 12.0 G, respectively, in the absence of explicit water molecules. However, on the basis of the Boltzmann average of the hfsc values of the various conformers, the predicted $a_{\beta\text{-H}}$ in the presence of water molecules overestimated the experimental $a_{\beta\text{-H}}$ by 1.4 G but this value was underestimated in the absence of water interaction by ~4 G. Since the calculated a_N did not change significantly for the conformers, I-A and II-B, and the $a_{\beta\text{-H}}$ only increased by ~1 G with explicit water molecules, reasonably good approximation of the hfsc's can therefore be

TABLE 4: Calculated Hyperfine Splitting Constants at the BHandHLYP/EPR-III (or PCM(water)/ BHandHLYP/ EPR-III) Level of Theory with Use of B3LYP/6-31G* Geometries of Various DMPO-O_2H Conformations and Their Complexes with Two Explicit Water Molecules

conformation	$\Delta G_{rel,298K}$	a_N	$a_{\beta\text{-H}}$	$a_{\gamma\text{-Ha}}$	$a_{\gamma\text{-Hb}}$	$a_{\gamma\text{-Hc}}$	$a_{\gamma\text{-Hd}}$
BHandHLYP/EPR-III//B3LYP/6-31G*							
gas phase							
I-A	0.0	14.0	7.9	−0.4	0.3	0.8	0.1
II-B	1.7	11.3	10.1	−0.3	−0.3	0.5	0.8
II-C	3.4	11.0	3.5	−0.2	−0.5	0.5	2.1
II-D	4.0	10.5	5.5	−0.2	−0.4	0.5	1.5
I-E	3.2	10.7	5.5	−0.2	−0.4	0.5	1.4
Boltzmann ave		**13.2**	**8.3**		**0.9**		
PCM(water)/BHandHLYP/EPR-III//B3LYP/6-31G*							
aqueous phase							
I-A	3.2	16.3	7.4	−0.5	0.2	0.9	0.1
II-B	0.0	13.7	12.0	−0.4	−0.5	0.5	0.9
II-C	0.0	13.6	4.2	−0.3	−0.6	0.5	2.4
II-D	0.8	13.2	6.5	−0.3	−0.5	0.5	1.7
I-E	0.6	13.2	6.6	−0.3	−0.5	0.5	1.5
Boltzmann ave		**13.5**	**7.6**		**1.6**		
PCM(water)/BHandHLYP/EPR-III//B3LYP/6-31G*							
aqueous phase							
I-A·$(H_2O)_2$	4.1	16.2	8.6	−0.5	0.2	0.7	0.1
II-B·$(H_2O)_2$	0.0	13.6	13.2	−0.4	−0.5	0.4	0.8
Boltzmann ave		**13.6**	**13.1**		**0.8**		
exptl		**14.3**	**11.7**		**1.3**		

achieved by using the most preferred isomer with the highest $a_{\beta\text{-H}}$ at the PCM(water)/BHandHLYP/EPR-III level in the absence of explicit water interaction.

c. Effect of the Hydroperoxyl Moiety Conformation. Table 4 shows that $a_{\beta\text{-H}}$ values vary significantly compared to a_N values for various conformers. The nature of this variation was further investigated by examining the sensitivity of $a_{\beta\text{-H}}$ to variations in the ∠N−C−O−O dihedral angle along the hydroperoxyl moiety and a similar study was done for a_N and a_γ as depicted in Figure 2. Oscillating $a_{\beta\text{-H}}$ values is evident during rotation along the $C_{ring}-O_{peroxyl}$ bond. The a_N and $a_{\gamma-H}$ values are less sensitive to the conformational changes of the hydroperoxyl moiety, for example, I-A gave a_N and α_γ values ranging from 9.0 to 12.1 G and 0.3 to 2.3 G, respectively, while $a_{\beta\text{-H}}$ exhibited the widest range with 2.6−10.9 G. Conformer II-B gave the same trend with a_N, $a_{\gamma-H}$, and $a_{\beta\text{-H}}$ values that range from 8.8 to 12.1, from 0.3 to 2.4, and from 3.0 to 11.0 G, respectively. As shown in Figure 2, the lowest potential energy for I-A gave the highest a_N, while $a_{\beta\text{-H}}$ was intermediate. The maximum $a_{\beta\text{-H}}$ was observed at the second lowest minima while the lowest $a_{\beta\text{-H}}$ was observed at the highest saddle point of the potential energy surface. Conformer II-B gave a more consistent trend in which the $a_{\beta\text{-H}}$ is maximum at the lowest potential energy, and vice versa. The high dependence of the $a_{\beta\text{-H}}$ on ∠N−C−O−O dihedral angle along the hydroperoxyl moiety can be explained through spin delocalization on the β-H at varying dihedral angles during conformational changes. Janzen[34] suggested that hyperconjugation of the β-H σ-orbital with the singly occupied molecular orbital (SOMO) of the N−O affects the magnitude of the $a_{\beta\text{-H}}$ according to the Heller and McConnell[35] eq 4:

$$a_{\beta\text{-H}} = \rho^N(K\cos^2\theta) \quad (4)$$

where K is constant, θ is the dihedral angle between the SOMO and CH σ-orbital ($\theta = 90° - \varphi$) (see Figure 3), and ρ^N is the spin density on nitrogen. Equation 3, however, only applies to β-H in the rotating conformations while β-H in our study is more of the rocking-type similar to that proposed by Morokuma and Fukui,[36] but studies showed that regardless of the type of conformational changes, i.e., rotating or rocking, low θ values always yield higher β-H hfsc.[36]

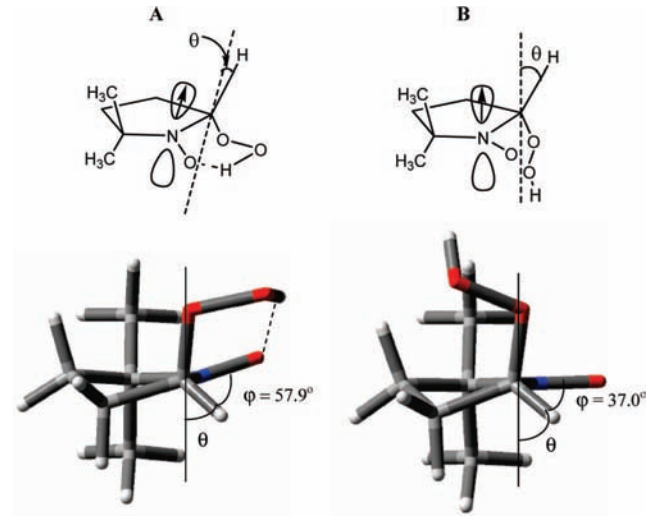

Figure 3. Most (A, left) and least (B, right) stable conformers of I-A (see Figure 1) at the B3LYP/6-31G* level showing the angle θ formed between the β-H and the SOMO of the nitrogen atom.

Examination of the most and least stable conformers for I-A, as A and B, respectively (see Figure 3), shows that H-bond interaction in A results in a higher ∠O−N−C−H dihedral angle ($\varphi = 57.9°$) compared to B with $\varphi = 37.0°$ when using the I-A conformer, while II-B gave ∠O−N−C−H of $\varphi = 47.3°$ and 37.2°, for the most and least stable conformers, respectively (figures not shown). Although the observed θ for A is much smaller than that for B, closer analysis of the conformational change from A → B shows that the ring conformation is only slightly changed as evidenced by the ∠C−N−C−H dihedral angle change from 138.8° to only 142.3°, respectively, indicating that the position of the β-H relative to the ring system is not much affected by rotation around the $C_{ring}-O_{peroxyl}$ bond. The change is more remarkable for ∠O−N−C−H as discussed above, which results in the slight pyramidalization of the nitrogen (Figure 3). There is no significant difference in the calculated a_N between conformers A and B, which indicates that the large difference in $a_{\beta\text{-H}}$ between A and B is not due to decreased spin density distribution on the nitrogen atom. It can therefore be reasonably assumed that although the $\cos^2\theta$ rule for β-H does not apply, the significant changes in the magnitude of $a_{\beta\text{-H}}$ could be angular dependent in which increase in the hyperconjugation of the CH σ-orbital with the singly occupied orbital (SOMO) increases the $a_{\beta\text{-H}}$. This hyperconjugative effect on the $a_{\beta\text{-H}}$ is further supported by the plot shown in Figure 4 demonstrating the direct proportionality of $a_{\beta\text{-H}}$ to the ∠O−N−C−H dihedral angle (φ) for both I-A and II-B isomers.

V. C5-Substituted Pyrroline *N*-Oxides

a. Conformational Search. The ∠N−C−C═O dihedral angles for the cis−trans isomers of AMPO-O_2H and EMPO-O_2H and ∠N−C−P═O angles DEPMPO-O_2H, respectively, were varied by using the most preferred ∠N−C−O−O dihedral angles obtained from DMPO-O_2H. Results show a potential energy profile at the B3LYP/6-31G* level that gives 1 minimum for the cis isomer of AMPO-O_2H and 4 minima for EMPO-O_2H or DEPMPO-O_2H (see Figure S24−S28 of the Supporting Information). For the trans adducts, 1 minimum was observed

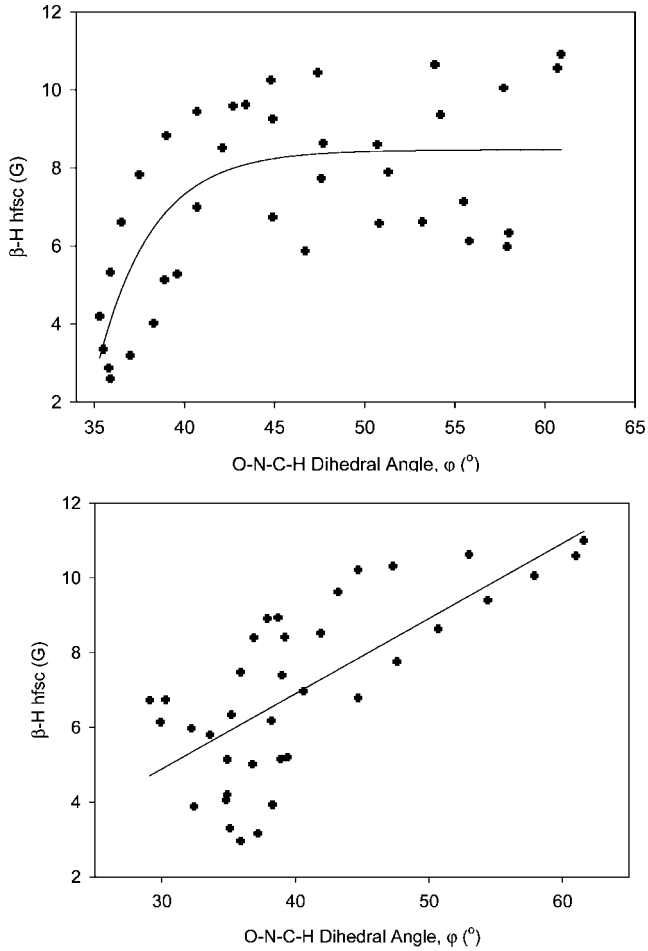

Figure 4. Dependence of β-hydrogen hfsc ($a_{\beta\text{-H}}$) on the ∠O−N−C−H dihedral angle (φ) in DMPO-O_2H conformers I-A (top) and II-B (bottom) at the B3LYP/6-31G* level of theory.

SCHEME 3: Schematic Representation of the ∠N−C−O−O (Φ) and ∠N−C−C(P)−O (Θ) Dihedral Angles Formed from the Rotations along the $C_{ring}-O_{peroxyl}$ and $C_{ring}-C_{carbonyl}$ (or $C_{ring}-P_{phosphoryl}$) Bonds, Respectively

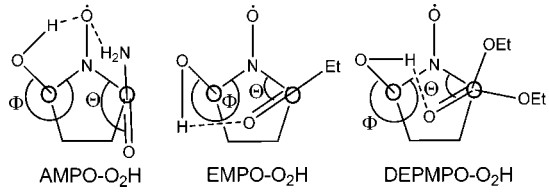

for AMPO-O_2H and 3 minima for EMPO-O_2H or DEPMPO-O_2H. The difference in the number of minima for AMPO-O_2H compared to EMPO-O_2H or DEPMPO-O_2H is due to the strong intramolecular H-bond interaction of the N−O group with the amide N−H giving ∠N−C−C═O dihedral angles of Θ = 143.0° and 140.1° for the cis and trans AMPO-O_2H, respectively, based on optimized geometries at the B3LYP/6-31G* level (see Scheme 3). The global minima for the cis adducts of EMPO-O_2H or DEPMPO-O_2H exhibited intramolecular H-bond interaction between the C═O or P═O and the hydroperoxyl-H, with ∠N−C−C═O and ∠N−C−P═O dihedral angles of Θ = 46.0° and 39.1°, respectively, based on optimized geometries. The ∠N−C−O−O dihedral angles of Φ = 282.7°, 73.3°, and 303.3° were also obtained based on the optimized global minima for cis-adducts of AMPO, EMPO, and DEPMPO, respectively. Since rotation along the $C_{ring}-C_{carbonyl}$ in CP-COMPO-O_2H is hindered, no potential energy plot as a function of ∠N−C−O−O dihedral angle was obtained.

Rotation along the $C_{ring}-O_{peroxyl}$ bond was performed and ∠N−C−O−O dihedral angles were plotted as a function of bottom-of-the-well energies without imposing conformational restrictions on the ester, amide, and phosphoryl groups (Figures S32−S39 in the Supporting Information). Substituent conformations at the cis position favor Θ = 136.5°, 60.2°, and 40.7°, while the trans isomers favor Θ = 140.1°, 101.4°, and 50.8°, for AMPO-O_2H, EMPO-O_2H, and DEPMPO-O_2H, respectively (see Scheme 3). The potential energy plots as a function of ∠N−C−O−O dihedral angles for the I and II conformational forms of *cis*-AMPO-O_2H, *cis*-EMPO-O_2H, *cis*-DEPMPO-O_2H, and *cis*-CPCOMPO-O_2H adducts gave a total of 6 minima for each adduct, similar to the trend observed for DMPO-O_2H. Each of the trans adducts also gave a total of 6 minima for the I and II conformational forms. Therefore, there are at least 12 minima for each adduct according to the potential energy plots as a function of ∠N−C−O−O dihedral angles.

In general, the relative free energies ($\Delta G_{rel,298K}$) at the PCM(water)/B3LYP/6-31+G**//B3LYP/6-31G* level of theory of the various adduct conformations show that the trans isomers are more preferred than the cis isomers by ∼2−6 kcal/mol except for CPCOMPO-O_2H in which the cis−trans isomers gave <1 kcal/mol energy difference (Table 5). This thorough conformational search on the adducts indicates the preference for the trans adducts, which is consistent with the extensive EPR analysis by Rockenbauer et al. for DEPMPO-O_2H.[37]

b. Prediction of Hyperfine Splitting Constants. The most stable I-A and II-B conformations for the *cis* and *trans* isomers of AMPO-O_2H, EMPO-O_2H, DEPMPO-O_2H, and CPCOMPO-O_2H were selected from the conformational search and further optimized at the B3LYP/6-31G* level of theory. Single-point calculations at the PCM(water)/BHandHLYP/EPR-III//B3LYP/6-31G* level were performed to obtain the hfsc values for a_N, $a_{\beta\text{-H}}$, and $a_{\gamma\text{-H}}$ as well as a_P in the case of DEPMPO-O_2H. Since calculation of hfsc's for DEPMPO-O_2H at the PCM(water)/BHandHLYP/EPR-III//B3LYP/6-31G* level was unsuccessful, single-point calculation at PCM(water)/BHandHLYP/6-31+G** was used as well for all the adducts and is shown in Table 5. Results show that in general, the calculated hfsc's at the PCM(water)/BHandHLYP/EPR-III level are in better agreement with the experimental hfsc values compared to PCM(water)/BHandHLYP/6-31+G**. Calculation of the hfsc values for DEPMPO-O_2H was unsuccessful at the PCM(water)/BHandHLYP/EPR-III level but it is expected that hfsc calculated at the BHandHLYP/6-31+G** will give a 1 G improvement at the PCM(water)/BHandHLYP/EPR-III level similar to that observed for the $O_2^{\bullet-}$ adducts of AMPO, EMPO, and CPCOMPO. Excellent agreement was obtained for a_N at the PCM(water)/BHandHLYP/EPR-III level except for *cis*-AMPO-O_2H in which the value was overestimated by ∼2.5 G based on the Boltzmann weighted hfsc, while the $a_{\beta\text{-H}}$ was underestimated by ∼2−4 G for the *cis*-AMPO-O_2H, *cis*-DEPMPO-O_2H, and CPCOMPO-O_2H. The $a_{\gamma\text{-H values}}$ for all the adducts and a_P for *cis*- and *trans*-DEPMPO-O_2H also gave good agreement with the experimental values. In general, the more preferred trans adducts gave better agreement to the experimental values than the cis adducts. Similar to the hfsc prediction for DMPO-O_2H but by Boltzmann averaging the most preferred diastereoisomers (i.e., trans isomers) at the PCM(water)/BHandHLYP/EPR-III//B3LYP/6-31G*, relevant hfsc's can now be predicted for C-5 substituted $O_2^{\bullet-}$ adducts with high accuracy by using a low cost compu-

TABLE 5: Relative Enthalpies, $H_{aq,298K}$, and Free Energies, $G_{aq,298K}$ (in kcal/mol), of Superoxide Radical Anion Adducts at the PCM(water)/B3LYP/6-31+G//B3LYP/6-31G* Level of Theory, and Their Respective Hyperfine Splitting Constants (G) at the PCM(water)/BHandHLYP/6-31+G**//B3LYP/6-31G* and PCM(water)/BHandHLYP/EPR-III//B3LYP/6-31G* (in parentheses) Levels**

	relative energies in water (kcal/mol)		predicted hyperfine splitting constants (G)				
nitrone-O_2H adducts	rel G	rel H	a_N	$a_{\beta\text{-H}}$	$a_{\gamma\text{-H1}}$	$a_{\gamma\text{-H2}}$	a_P
AMPO-O_2H							
cis-1	3.8	3.5	16.0 (15.4)	6.9 (7.3)	0.6 (0.6)	0.7 (0.7)	
cis-2	5.9	4.6	15.3 (14.7)	7.0 (7.3)	1.0 (1.0)	1.0 (1.0)	
Boltzmann ave (cis)			**16.0 (15.4)**	**6.9 (7.3)**	**0.6 (0.6)**	**0.7 (0.7)**	
trans-1	2.8	2.7	15.5 (14.9)	7.2 (7.5)	0.8 (0.8)	0.6 (0.5)	
trans-2	0.0	0.0	14.5 (13.8)	11.0 (11.5)	0.4 (0.4)	0.9 (0.9)	
Boltzman ave (trans)			**14.5 (13.8)**	**11.0 (11.5)**	**0.4 (0.4)**	**0.9 (0.9)**	
exptl[19] 80%			**13.0**	10.8			
exptl[19] 20%			**13.1**	**12.5**	**1.8**		
EMPO-O_2H							
cis-1	1.6	0.5	14.1 (13.1)	13.8 (14.4)	0.7 (0.8)	0.2 (0.2)	
cis-2	2.6	1.8	16.3 (15.7)	11.7 (12.2)	0.2 (0.2)	0.1 (0.1)	
cis-3	1.8	0.0	13.8 (13.1)	7.9 (8.2)	1.2 (1.3)	0.9 (0.9)	
Boltzmann ave (cis)			**14.2 (13.4)**	**11.3 (11.8)**	**0.8 (0.9)**	**0.5 (0.5)**	
trans-1	2.6	1.7	16.1 (15.4)	7.5 (7.7)	0.8 (0.8)	0.8 (0.9)	
trans-2	0.0	0.0	14.2 (13.4)	12.2 (12.6)	0.3 (0.3)	0.7 (0.7)	
trans-3	2.7	1.8	16.1 (15.4)	7.5 (7.8)	0.8 (0.8)	0.8 (0.9)	
Boltzmann ave (trans)			**14.2 (13.4)**	**12.1 (12.5)**	**0.3 (0.3)**	**0.7 (0.7)**	
exptl[39] 59%			**13.1**	**11.7**	**n/a[a]**		
exptl[39] 41%			**13.1**	**9.3**	**n/a[a]**		
DEPMPO-O_2H							
cis-1	3.3	0.8	14.3	1.8	2.1	1.0	38.1
cis-2	3.7	2.3	14.3	14.0	0.1	0.3	52.2
Boltzmann ave (cis)			**14.3**	**5.7**	**1.5**	**0.8**	**42.6**
trans-1	3.7	2.4	15.7	7.9	0.1	0.8	44.9
trans-2	0.0	0.0	14.0	12.4	0.5	0.2	47.4
Boltzmann ave (trans)			**14.0**	**12.4**	**0.5**	**0.2**	**47.4**
exptl[40] 50%			**13.4**	**11.9**	0.8		**52.5**
exptl[40] 50%			**13.2**	**10.3**	0.9		**48.5**
CPCOMPO-O_2H							
cis-1	0.0	0.0	13.8 (13.0)	6.8 (7.1)	1.3 (1.3)	1.1 (1.1)	
cis-2	0.6	1.5	16.3 (15.7)	6.0 (6.3)	0.2 (0.3)	0.9 (0.9)	
Boltzmann ave			**14.4 (13.7)**	**6.6 (6.9)**	**1.0 (1.0)**	**1.0 (1.0)**	
trans-1	0.3	1.4	15.6 (14.9)	8.2 (8.6)	0.5 (0.5)	0.8 (0.8)	
exptl[20] 62%			**13.0**	**10.0**	**1.5**		
exptl [20] 17%			**13.1**	**11.5**	**1.1**		

[a] Not available.

tational method and without taking into account the explicit water interaction that is tedious to implement.

c. Sensitivity of Spin−Nuclei Coupling to the Substituent Conformational Changes. Table S3 in the Supporting Information shows the complete list of calculated hfsc's for nitrogen, β- and γ-hydrogen atoms and their ranges from 360° rotation along the $C_{ring}-O_{peroxyl}$, $C_{ring}-C_{carbonyl}$, and $C_{ring}-P_{phosphoryl}$ bonds at the B3LYP/6-31G* level of theory. Similar to that observed for DMPO-O_2H, the highest change in hfsc was observed on the $a_{\beta\text{-H}}$ compared to a_N and the $a_{\gamma\text{-H}}$ values as indicated by the magnitude of the Δa_x values shown in Table 6. The hfsc values for phosphorus atom in DEPMPO-O_2H were also found to be very sensitive to the conformational changes of the phosphoryl and hydroperoxyl moieties with Δa_P values that range from ~10 to 30 G (see Table S3 in the Supporting Information for the effect of conformational changes from the phosphoryl group on a_P). The high $a_{\beta\text{-H}}$ values observed for all the C-5 substituted adducts were due to the high φ (or low θ) ∠O−N−C−H dihedral angle that favors hyperconjugation between the CH σ-orbital and the SOMO orbital. Figures S9−S31 in the Supporting Information show the various φ obtained with their respective $a_{\beta\text{-H}}$ values during rotation along the $C_{ring}-O_{peroxyl}$ and $C_{ring}-C_{carbonyl}$ (or $C_{ring}-C_{phosphoryl}$) bonds demonstrating the direct proportionality between φ and $a_{\beta\text{-H}}$ for some of the conformations.

VI. Conclusions

The B3LYP/6-31G* level of theory gave bottom-of-the-well energy value that is close to that obtained with the most accurate method CBS-QB3 and provided a low-cost yet accurate estimate of the reaction energies as compared to the other methods and basis sets explored in this study. Exhaustive conformational search of DMPO-O_2H yielded two global minima for the I- and II-type conformations. Using the B3LYP/6-31G* preferred geometries for the I- and II-type conformations of DMPO-O_2H, BHandHLYP gave the best approximations of the hfsc's using the basis sets EPR-II or EPR-III in both gas and aqueous phases. The effect of explicit water interaction on the magnitude of hfsc's was negligible and that hfsc's can be reasonably predicted with high accuracy using the most preferred conformation and by only accounting for the bulk dielectric effect of water. The effect of rotation along the $C_{ring}-O_{peroxyl}$ bond for DMPO-O_2H shows significant change in the magnitude of $a_{\beta\text{-H}}$ and only small changes on the $a_{\gamma-H}$ and a_N. This high sensitivity of $a_{\beta\text{-H}}$ to conformational changes of the hydroperoxyl moiety is due to

TABLE 6: Calculated Range of Hyperfine Splitting Constants (hfsc) (in G) for Nitrogen, β-Hydrogen, and γ-Hydrogen Atoms of Various Preferred Adduct Conformations Calculated at the B3LYP/6-31G* Level of Theory[a]

nitrone-O_2H adducts	a_N	$a_{\gamma\text{-Ha}}$	$a_{\gamma\text{-Hb}}$	$a_{\gamma\text{-Hc}}$	$a_{\gamma\text{-Hd}}$	$a_{\beta\text{-H}}$	misc.
DMPO-I	8.84−12.05 (3.21)	−0.34−0.12 (0.22)	−0.36−0.34(0.71)	0.52−1.69 (1.17)	0.28−2.45(2.18)	2.96−11.0 (8.04)	
DMPO-II	8.97−12.06 (3.08)	−0.34−0.12 (0.22)	−0.29−0.35(0.63)	0.53−1.64 (1.11)	0.29−2.25(1.96)	2.60−10.92 (8.32)	
							$a_{N(amide)}$
AMPO-cis-I	9.78−12.19 (2.41)	−0.55−0.31 (0.25)	−0.36−0.18(0.18)	0.83−2.15 (1.31)	0.46−1.34(0.88)	1.16−9.64 (8.48)	0.84−1.39 (0.55)
AMPO-trans-II	9.62−10.65 (1.02)	−0.35−0.16 (0.19)	−0.19−0.13(0.32)	0.50−1.40 (0.89)	0.89−2.26(1.37)	3.51−10.19 (6.67)	1.43−1.96 (0.54)
EMPO-cis-I	8.86−11.45 (2.58)	−0.34−0.04 (0.30)	0.18−1.28(1.09)	0.04−1.40 (1.36)	−0.28−0.31(0.59)	6.14−16.39 (10.25)	
EMPO-trans-II	8.59−10.62 (2.04)	−0.31−0.01 (0.30)	−0.30−0.80(1.11)	0.60−1.63 (1.03)	−0.05−2.39(2.44)	3.67−11.08 (7.41)	
							a_P
DEPMPO-cis-I	8.75−11.35 (2.60)	−0.53−0.28 (0.24)	−0.41−1.16(1.57)	0.25−2.47 (2.21)	−0.32−1.66(1.98)	0.72−16.83 (16.11)	37.66−54.22 (16.56)
DEPMPO-trans-II	8.93−10.47 (1.53)	−0.44−0.26 (0.18)	−0.47−0.19(0.66)	0.49−1.40 (0.92)	0.22−2.32(2.10)	3.83−11.61 (7.78)	39.51−49.65 (10.14)
CPCOMPO-cis-I	8.45−12.05 (3.60)	−0.49−0.08 (0.57)	−0.33−0.21(0.54)	0.71−2.71 (2.01)	0.50−1.61(1.11)	1.81−8.86 (7.05)	
CPCOMPO-trans-I	8.58−11.38 (2.80)	−0.41−0.08 (0.33)	−0.21−0.57(0.78)	0.46−1.44 (0.98)	0.13−2.05(1.92)	4.01−11.71 (7.69)	

[a] Values in parentheses are Δa_x values ($a_{maximum} - a_{minimum}$) in G. (See Table S3 in the Supporting Information for the complete list.)

the angular dependence of the hyperconjugation of the β-H σ-orbital with the SOMO.

An extensive conformational search was also carried out on C-5 substituted $O_2^{\bullet-}$ adducts of AMPO, EMPO, DEPMPO, and CPCOMPO. The preferred geometries show strong intramolecular interaction of the hydroperoxyl-H with the phosphoryl-O, carbonyl-O, and nitroxyl-O for the cis- and trans-adducts. The hfsc's were predicted for all the preferred cis- and trans-adducts and results show very good agreement of the predicted hfsc's to the experimental values by using the PCM(water)/BHandHLYP/EPR-III//B3LYP/6-31G* level of theory and by Boltzmann weighing of the hfsc's of the preferred trans conformations without taking into account the explicit water interaction. Similar to that observed for DMPO-O_2H, the $a_{\beta\text{-H}}$ was found to be sensitive to conformational changes from rotations along the $C_{ring}-O_{peroxyl}$ and $C_{ring}-C_{carbonyl}$ (or $C_{ring}-C_{phosphoryl}$) bonds of the various adducts and that the hyperconjugation arising from these bond rotations has a major effect on the magnitude of the $a_{\beta\text{-H}}$.

Acknowledgment. This work is supported by NIH grants HL81248 and HL38324. The Ohio Supercomputer Center (OSC) is acknowledged for generous computational support of this research. The authors thank Prof. Christopher Hadad for helpful suggestions.

Supporting Information Available: Cartesian coordinates for all the compounds and miscellaneous plots. This material is available free of charge via the Internet at http://pubs.acs.org.

References and Notes

(1) Janzen, E. G. *Acc. Chem. Res.* **1971**, *4*, 31. Janzen, E. G.; Haire, D. L. *Adv. Free Radical Chem.* **1990**, *1*, 253. Villamena, F. A.; Zweier, J. L. *Antioxid. Redox Signaling* **2004**, *6*, 619.

(2) Bhattacharjee, S.; Deterding, L. J.; Jiang, J.; Bonini, M. G.; Tomer, K. B.; Ramirez, D. C.; Mason, R. P. *J. Am. Chem. Soc.* **2007**, *129*, 13493. Haywood, R.; Rogge, F.; Lee, M. *Free Radical Biol. Med.* **2008**, *44*, 990. Kennett, E. C.; Davies, M. J. *Free Radical Biol. Med.* **2007**, *42*, 1278. Rees, M. D.; Davies, M. J. *J. Am. Chem. Soc.* **2006**, *128*, 3085. Velayutham, M.; Muthukumaran, R. B.; Sostaric, J. Z.; McCraken, J.; Fishbein, J. C.; Zweier, J. L. *Free Radical Biol. Med.* **2007**, *43*, 1076. Zhu, B.-Z.; Kalyanaraman, B.; Jiang, G.-B. *Proc. Natl. Acad. Sci. U.S.A.* **2007**, *104*, 17575. Zhu, B.-Z.; Zhao, H.-T.; Kalyanaraman, B.; Liu, J.; Shan, G.-Q.; Du, Y.-G.; Frei, B. *Proc. Natl. Acad. Sci. U.S.A.* **2007**, *104*, 3698.

(3) Chen, C.-L.; Zhang, L.; Yeh, A.; Chen, C.-A.; Green-Church, K. B.; Zweier, J. L.; Chen, Y.-R. *Biochemistry* **2007**, *46*, 5754. Chen, Y.-R.; Chen, C.-L.; Yeh, A.; Liu, X.; Zweier, J. L. *J. Biol. Chem.* **2006**, *281*, 13159. Piacenza, L.; Irigoin, F.; Alvarez, M. N.; Peluffo, G.; Taylor, M. C.; Kelly, J. M.; Wilkinson, S. R.; Radi, R. *Biochem. J.* **2007**, *403*, 323.

(4) Bosnjakovic, A.; Kadirov, M. K.; Schlick, S. *Res. Chem. Intermed.* **2007**, *33*, 677. Danilczuk, M.; Bosnjakovic, A.; Kadirov, M. K.; Schlick, S. *J. Power Sources* **2007**, *172*, 78. Bosnjakovic, A.; Schlick, S. *J. Phys. Chem. B* **2006**, *110*, 10720.

(5) Ionita, P.; Conte, M.; Gilbert, B. C.; Chechik, V. *Org. Biomol. Chem.* **2007**, *5*, 3504. Babu, S.; Velez, A.; Wozniak, K.; Szydlowska, J.; Seal, S. *Chem. Phys. Lett.* **2007**, *442*, 405. Kagan, V. E.; Tyurina, Y. Y.; Tyurin, V. A.; Konduru, N. V.; Potapovich, A. I.; Osipov, A. N.; Kisin, E. R.; Schwegler-Berry, D.; Mercer, R.; Castranova, V.; Shvedova, A. A. *Toxicol. Lett.* **2006**, *165*, 88.

(6) Fu, H.; Zhang, L.; Zhang, S.; Zhu, Y.; Zhao, J. *J. Phys. Chem. B* **2006**, *110*, 3061.

(7) Xiao, G.; Wang, X.; Li, D.; Fu, X. *J. Photochem. Photobiol., A* **2008**, *193*, 213. Chang, Q.; He, H.; Zhao, J.; Yang, M.; Qu, J. *Environ. Sci. Technol.* **2008**, *42*, 1699. Yu, J. C.; Ho, W.; Yu, J.; Yip, H.; Wong, P. K.; Zhao, J. *Environ. Sci. Technol.* **2005**, *39*, 1175.

(8) Zeng, Z.; Zhou, J.; Zhang, Y.; Qiao, R.; Xia, S.; Chen, J.; Wang, X.; Zhang, B. *J. Phys. Chem. B* **2007**, *111*, 2688. Rajendran, M.; Inbaraj, J. J.; Gandhidasan, R.; Murugesan, R. *J. Photochem. Photobiol., A* **2006**, *182*, 67. Mroz, P.; Pawlak, A.; Satti, M.; Lee, H.; Wharton, T.; Gali, H.; Sarna, T.; Hamblin, M. R. *Free Radical Biol. Med.* **2007**, *43*, 711.

(9) Finkelstein, E.; Rosen, G. M.; Rauckman, E. J. *J. Am. Chem. Soc.* **1980**, *102*, 4994.

(10) Olive, G.; Mercier, A.; Le Moigne, F.; Rockenbauer, A.; Tordo, P. *Free Radical Biol. Med.* **2000**, *28*, 403.

(11) Frejaville, C.; Karoui, H.; Tuccio, B.; Le Moigne, F.; Culcasi, M.; Pietri, S.; Lauricella, R.; Tordo, P. *J. Chem. Soc., Chem. Commun.* **1994**, 1793.

(12) Steadman, R.; Petersen, M. M.; Topley, N.; Williams, D.; Matthews, N.; Spur, B.; Williams, J. D. *J. Immunol.* **1990**, *144*, 2712. Pechtelidou, A.; Beis, I.; Gaitanaki, C. *Mol. Cell. Biochem.* **2008**, *309*, 177. Paul, K.; Bauer, G. *Anticancer Res.* **2001**, *21*, 3237. Chiaramonte, R.; Bartolini, E.; Riso, P.; Calzavara, E.; Erba, D.; Testolin, G.; Comi, P.; Sherbet, G. V. *J. Cell. Biochem.* **2001**, *82*, 437.

(13) Halliwell, B.; Gutteridge, J. M. C. *Free Radicals in Biology and Medicine*, 4th ed.; Oxford University: New York, 2007.

(14) Villamena, F. A.; Hadad, C. M.; Zweier, J. L. *J. Phys. Chem. A* **2003**, *107*, 4407. Villamena, F. A.; Hadad, C. M.; Zweier, J. L. *J. Am. Chem. Soc.* **2004**, *126*, 1816. Villamena, F. A.; Hadad, C. M.; Zweier, J. L. *J. Phys. Chem. A* **2005**, *109*, 1662.

(15) Villamena, F. A.; Merle, J. K.; Hadad, C. M.; Zweier, J. L. *J. Phys. Chem. A* **2005**, *109*, 6089.

(16) Villamena, F. A.; Merle, J. K.; Hadad, C. M.; Zweier, J. L. *J. Phys. Chem. A* **2005**, *109*, 6083.

(17) Villamena, F. A.; Merle, J. K.; Hadad, C. M.; Zweier, J. L. *J. Phys. Chem. A.* **2007**, *111*, 9995.

(18) Villamena, F. A.; Xia, S.; Merle, J. K.; Lauricella, R.; Tuccio, B.; Hadad, C. M.; Zweier, J. L. *J. Am. Chem. Soc.* **2007**, *129*, 8177.

(19) Villamena, F. A.; Rockenbauer, A.; Gallucci, J.; Velayutham, M.; Hadad, C. M.; Zweier, J. L. *J. Org. Chem.* **2004**, *69*, 7994.

(20) Han, Y.; Tuccio, B.; Lauricella, R.; Rockenbauer, A.; Zweier, J. L.; Villamena, F. A. *J. Org. Chem.* **2008**, *73*, 2533.

(21) Clement, J.-L.; Ferre, N.; Siri, D.; Karoui, H.; Rockenbauer, A.; Tordo, P. *J. Org. Chem.* **2005**, *70*, 1198.

(22) Rosen, G. M.; Beselman, A.; Tsai, P.; Pou, S.; Mailer, C.; Ichikawa, K.; Robinson, B. H.; Nielsen, R.; Halpern, H. J.; MacKerell, A. D., Jr *J. Org. Chem.* **2004**, *69*, 1321.

(23) Rockenbauer, A.; Clement, J.-L.; Culcasi, M.; Mercier, A.; Tordo, P.; Pietri, S. *J. Phys. Chem. A* **2007**, *111*, 4950.

(24) Saracino, G. A. A.; Tedeschi, A.; D'Errico, G.; Improta, R.; Franco, L.; Ruzzi, M.; Corvaia, C.; Barone, V. *J. Phys. Chem. A* **2002**, *106*, 10700.

(25) Allouch, A.; Lauricella, R. P.; Tuccio, B. N. *Mol. Phys.* **2007**, *105*, 2017. Finkelstein, E.; Rosen, G. M.; Rauckman, E. J. *Arch. Biochem. Biophys.* **1980**, *200*, 1.

(26) Behar, D.; Czapski, G.; Rabani, J.; Dorfman, L. M.; Schwarz, H. A. *J. Phys. Chem.* **1970**, *74*, 3209.

(27) Frischt, M. J.; Trucks, G. W.; Schlegel, H. B.; Scuseria, G. E.; Robb, M. A.; Cheeseman, J. R.; Montgomery, J. A., Jr.; Vreven, T.; Kudin, K. N.; Burant, J. C.; Millam, J. M.; Iyengar, S. S.; Tomasi, J.; Barone, V.; Mennucci, B.; Cossi, M.; Scalmani, G.; Rega, N.; Petersson, G. A.; Nakatsuji, H.; Hada, M.; Ehara, M.; Toyota, K.; Fukuda, R.; Hasegawa, J.; Ishida, M.; Nakajima, T.; Honda, Y.; Kitao, O.; Nakai, H.; Klene, M.; Li, X.; Knox, J. E.; Hratchian, H. P.; Cross, J. B.; Bakken, V.; Adamo, C.; Jaramillo, J.; Gomperts, R.; Stratmann, R. E.; Yazyev, O.; Austin, A. J.; Cammi, R.; Pomelli, C.; Ochterski, J. W.; Ayala, P. Y.; Morokuma, K.; Voth, G. A.; Salvador, P.; Dannenberg, J. J.; Zakrzewski, V. G.; Dapprich, S.; Daniels, A. D.; Strain, M. C.; Farkas, O.; Malick, D. K.; Rabuck, A. D.; Raghavachari, K.; Foresman, J. B.; Ortiz, J. V.; Cui, Q.; Baboul, A. G.; Clifford, S.; Cioslowski, J.; Stefanov, B. B.; Liu, G.; Liashenko, A.; Piskorz, P.; Komaromi, I.; Martin, R. L.; Fox, D. J.; Keith, T.; Al-Laham, M. A.; Peng, C. Y.; Nanayakkara, A.; Challacombe, M.; Gill, P. M. W.; Johnson, B.; Chen, W.; Wong, M. W.; Gonzalez, C.; Pople, J. A. *Gaussian 03*; Gaussian, Inc: Pittsburgh, PA, 2003.

(28) Krenske, E. H.; Schiesser, C. H. *Org. Biomol. Chem.* **2008**, *6*, 854.

(29) (a) Labanowski, J. W.; Andzelm, J. *Density Functional Methods in Chemistry*;Springer: New York, 1991. Parr, R. G.; Yang, W. *Density Functional Theory in Atoms and Molecules*; Oxford University Press: New York, 1989.

(30) Becke, A. D. *Phys. Rev.* **1988**, *38*, 3098. Lee, C.; Yang, W.; Parr, R. G. *Phys. Rev. B* **1988**, *37*, 785. Becke, A. D. *J. Chem. Phys.* **1993**, *98*, 1372. Hehre, W. J.; Radom, L.; Schleyer, P. V.; Pople, J. A. *Ab Initio Molecular Orbital Theory*; John Wiley & Sons: New York, 1986.

(31) Cirujeda, J.; Vidal-Gancedo, J.; Jürgens, O.; Mota, F.; Novoa, J. J.; Rovira, C.; Veciana, J. *J. Am. Chem. Soc.* **2000**, *122*, 11393.

(32) Tomasi, J.; Persico, M. *Chem. Rev.* **1994**, *94*, 2027. Cossi, M.; Barone, V.; Cammi, R.; Tomasi, J. *Chem. Phys. Lett.* **1996**, *255*, 327. Barone, V.; Cossi, M.; Tomasi, J. *J. Chem. Phys.* **1997**, *107*, 3210. Barone, V.; Cossi, M.; Tomasi, J. *J. Comput. Chem.* **1998**, *19*, 404. Cossi, M.; Barone, V. *J. Chem. Phys.* **1998**, *109*, 6246.

(33) *Spartan'04*; Wavefunction, Inc., Irvine, CA, 2004.

(34) Janzen, E. G. Stereochemistry of Nitroxides. In *Topics in Stereochemistry*; Allinger,L. L., Eliel, E. L., Eds.; Wiley-Interscience: New York, 1971; Vol. *6*, p 186.

(35) Heller, C.; McConnell, M. *J. Chem. Phys.* **1960**, *32*, 1535.

(36) Morokuma, K.; Fukui, K. *Bull. Chem. Soc. Jpn.* **1963**, *36*, 534.

(37) Rockenbauer, A.; Clement, J.-L.; Culcasi, M.; Mercier, A.; Tordo, P.; Pietri, S. *J. Phys. Chem. A* **2007**, *111*, 4950.

(38) Tsai, P.; Marra, J. M.; Pou, S.; Bowman, M. K.; Rosen, G. M. *J. Org. Chem.* **2005**, *70*, 7093.

(39) Tsai, P.; Ichikawa, K.; Mailer, C.; Pou, S.; Halpern, H. J.; Robinson, B. H.; Nielsen, R.; Rosen, G. M. *J. Org. Chem.* **2003**, *68*, 7811.

(40) Frejaville, C.; Karoui, H.; Tuccio, B.; Le Moigne, F.; Culcasi, M.; Pietri, S.; Lauricella, R.; Tordo, P. *J. Med. Chem.* **1995**, *38*, 258.

JP8070579